metals

Article

Effect of the Addition of Cu and Al on the Microstructure, Phase Composition and Properties of a Ti-6Al-4V Alloy Obtained by Selective Laser Melting

Galina M. Zeer [1,*], Yuri I. Gordeev [1], Elena G. Zelenkova [1], Artur K. Abkaryan [1], Evgeny V. Gerasimov [1,2], Mikhail Yu. Kuchinskii [1] and Sergey M. Zharkov [1,3,*]

1 Siberian Federal University, 79 Svobodny Ave., Krasnoyarsk 660041, Russia; ygordeev@sfu-kras.ru (Y.I.G.); ezelenkova@sfu-kras.ru (E.G.Z.); abkaryan_artur@mail.ru (A.K.A.); gerasimov24rus@mail.ru (E.V.G.); mkuchinskiy@sfu-kras.ru (M.Y.K.)
2 LLC «Polihrom», Dubrovinskogo, 58/78, Krasnoyarsk 660049, Russia
3 Kirensky Institute of Physics, Federal Research Center KSC SB RAS, Akademgorodok 50/38, Krasnoyarsk 660036, Russia
* Correspondence: gzeer@sfu-kras.ru (G.M.Z.); zharkov@iph.krasn.ru (S.M.Z.)

Abstract: The present study considers the samples of an Ti-6Al-4V alloy obtained by selective laser melting with the addition of a 10% Cu-Al powder mixture. The microstructure, elemental composition and phase composition, as well as the physico-chemical properties, have been investigated by the methods of electron microscopy, X-ray phase analysis, and bending testing. The obtained samples have a relative density of 98.5 ± 0.1%. The addition of the Cu-Al powder mixture facilitates supercooling during crystallization and solidification, which allows decreasing the size and changing the shape of the initial β-Ti grains. The constant cooling rate of the alloy typical for the SLM technology has been shown to be able to prevent martensitic transformation. The formation of a structure that consists of β-Ti grains, a dispersed eutectoid mixture of α-Ti and Ti_2Cu grains, and a solid solution of Al in Cu has been revealed. In the case of doping by the 10% Cu-Al mixture, the physico-mechanical properties are improved. The hardness of the samples amounts to 390 HRC, with the bending strength being 1550 ± 20 MPa and deformation of 3.5 ± 0.2%. The developed alloy can be recommended for applications in the production of parts of jet and car engines, implants for medicine, and corrosion-resistant parts for the chemical industry.

Keywords: titanium alloys; Ti-6Al-4V; powders; additive technologies; selective laser melting; microstructure; physico-mechanical properties

Citation: Zeer, G.M.; Gordeev, Y.I.; Zelenkova, E.G.; Abkaryan, A.K.; Gerasimov, E.V.; Kuchinskii, M.Y.; Zharkov, S.M. Effect of the Addition of Cu and Al on the Microstructure, Phase Composition and Properties of a Ti-6Al-4V Alloy Obtained by Selective Laser Melting. *Metals* **2024**, *14*, 991. https://doi.org/10.3390/met14090991

Academic Editor: Eric Hug

Received: 24 July 2024
Revised: 10 August 2024
Accepted: 29 August 2024
Published: 30 August 2024

1. Introduction

Selective laser melting (SLM) is one of the technologies for the production of 3D items, including those of rather complex shapes. SLM involves layer-by-layer selective deposition of an initial material using a laser. Powders and powder mixtures are used as an initial material. The SLM technology is characterized by a number of significant advantages compared to similar techniques: a large working area allows us to obtain items of a rather large size, with carefully elaborated smaller elements and a sufficiently good quality of the surface [1–3]. The peculiarity of the SLM technology is residual porosity and defects of shape of the outer surface, which leads to the necessity of post-processing [4,5]. Moreover, upon cooling, the layers undergo shrinkage with the increasing inner strain, which can result in the deformation of the item and in the formation of cracks [6,7]. In the fabrication of products by the SLM method, use is made of metal powders and a wide range of powder alloys based on iron, nickel, titanium, aluminum, and cobalt. The powders have to be homogeneous in their chemical composition, include particles of spherical shape, and be characterized by high fluidity and packing degree [8–10]. In the samples obtained by the

SLM technology under the conditions of highly localized melting and fast solidification, pores are formed due to low fluidity and agglomeration of powders, their non-spherical shape, as well as non-uniform packing of particles in a layer occurring when the material is loaded into the melting zone [6,11].

In the application of the SLM technology, the alloy Ti-6Al-4V is a popular material [12–16]. The alloy is used in the production of fans of jet engines, engine valves in cars, knee and hip implants in biomedicine, as well as in the fabrication of corrosion-resistant pipes for the chemical industry [16]. Samples obtained by SLM technology have a complex structure, frequently due to the prevailing needle-like α'-phase, which occurs in columnar grains of the β-phase, which results in low plasticity and impact strength of the material [17]. It is found that during the formation of the material there occurs an anisotropy of properties between the vertically and horizontally deposited samples, with a cyclic elastoplastic anisotropy being observed [18–20]. Alloys doped with copper are promising for investigation. The titanium-based copper-containing alloy formed is shown to have good mechanical properties [7,21–27], resistance to corrosion [28,29], and antibacterial properties [29–31]. The disadvantage of adding Cu to this alloy is connected with its tendency towards the formation of an intermetallic compound Ti_2Cu, resulting in increased fragility [23,26,27,32,33].

Traditional casting is used to produce Ti-6Al-4V alloys doped with copper; upon equilibrium solidification, there occurs the segregation of Cu with pores and large grains being formed [21,33]. There are also technologies for obtaining copper-doped alloys using electron beam additive manufacturing with the simultaneous feeding of two different metallic wires. The increase in the copper content in the alloy from 0.6 to 9.7 wt.% resulted in the size reduction of the initial columnar β-Ti grains and their transformation to equiaxed ones [32]. This effect is due to the impact of copper on the accelerated development of the area of constitutional supercooling when grains are generated and formed.

In the case of additive manufacturing Ti–8.5% Cu, the area of constitutional supercooling is eight times larger in size as compared to Ti-6Al-4V, subjected to the same conditions of laser treatment. Sufficient constitutional supercooling can efficiently compensate for the impact of the high heat gradient and provides an opportunity for heterogeneous nucleation in the constitutional supercooling area and for achieving the complete transformation from the columnar β-Ti grain structure to the equiaxed one. The larger the amount of dissolved copper, the faster constitutional supercooling occurs and, consequently, the formation of an equiaxed grain of the β-phase accompanied by its decrease in size [5,26,27,32].

The alloy Ti-6Al-4V was chosen as the main component for this research since it has excellent mechanical and corrosion-resistant properties. The addition of the Cu-Al mixture to the Ti-6Al-4V powder allows the formation of a phase of an Al solid solution in Cu, which strengthens the eutectoid mixture (α-Ti + Ti_2Cu). The aim of this study is to investigate the impact of doping the alloy Ti-6Al-4V obtained by the SLM technology with the mixture of Cu and Al powders on the microstructure, phase-formation, and physico-mechanical properties (porosity, binding strength, and Young's modulus).

2. Materials and Methods

Samples of two types were used (those of rectangular section, with a width of 5 mm, a height of 5 mm, and a length of 55 mm; and cylindrical ones, with a height of 10 mm and a diameter of 10 mm) in the amount of 10 samples per each dimension type. The printer ASTRA 420 [34] produces the diameter of the spot of 60–2000 μm, with the time of focusing being less than 0.2 sec and with there being a possibility to change the power from 100 to 500 W for the IR laser with the wavelength of 1080 nm. For building various items, the printer allows reaching rates of 15 cm^3/m. The application of the powder is carried out with the step of 1μm, with the build chamber size being 420 × 420 × 280 mm and the medium being the vacuum or inert atmosphere (Ar).

The powders were mixed in a ball mill (RETSCH MM 400, Haan, Germany) at a vibration frequency of 30 s^{-1} in two steps for 50 min. Grinding balls were not used since it was necessary to prepare a uniform mixture without additional grinding of the initial powders.

The microstructure in the mode of backscattered electrons (BSE) and secondary electrons (SE) was investigated by the method of scanning electron microscopy (SEM) with an electron microscope JSM-7001F (JEOL, Tokyo, Japan) equipped with a system of microanalysers, Oxford Instruments (Abingdon, UK). The elemental composition of the phases was determined at certain points and across the area. The application of the BSE method allows us to obtain images of phases in the shades of the gray color, where the phases that include heavier elements have the light-gray color and the phases that include lighter elements are dark gray. The SE method gives information about the morphology of the sample surface. For the investigation of the microstructure and elemental composition on the surface of the samples, cross sections were made with the sequential application of abrasive paper (400, 800, 1200, and 2400 grit) and polishing using diamond suspension with a grain size of 0–1 μm and 0–0.5 μm on the installation BUEHLER: Beta Grinder-polisher, Vector Power Head (Stuttgart, Germany). For revealing the structure, the cross-sections were etched with the Kroll's reagent (4 mL HF, 10 mL HNO_3, and 86 mL H_2O).

The phase composition of the samples was determined with an X-ray diffractometer Bruker D8 (Karlsruhe, Germany) with a linear detector VANTEC equipped with CuKα-radiation with the following parameters: step—0.02°/step, angle range—2θ from 10° to 90°, and accumulation time—1 s/step.

The density of the samples was estimated by the method of hydrostatic weighing using an analytical scale METTLER TOLEDO XP 205 (Greifensee, Switzerland) equipped with a special module and software for density calculation. The values of density were obtained with an accuracy of up to 10^{-4} g/mm^3. The porosity was calculated using the formula $P = (1 - \rho/\rho_c) \times 100\%$, where ρ is the measured sample density; ρ_c is the density of the compact material 90%(Ti-6Al-4V)-10%(95%Cu-5%Al). $\rho_c = C_1 \times \rho_1 + C_2 \times \rho_2 + C_3 \times \rho_3$, where C is the amount, %; ρ is the density, g/mm^3 of the components of the samples Ti-6Al-4V, Cu, and Al, respectively.

The bend tests were carried out with a universal testing machine, Tinius Olsen H25KT (Kongsberg, Norway), using the three-point bend method. A localized load is applied on a sample located on two supports. After the post-processing, the sizes of the samples corresponded to the standard ISO: length of 50 mm; width of 10.0 ± 0.1 mm; height of 5.0 ± 0.1 mm. The bending strength and Young's modulus were calculated using the special software Horizon, including the built-in library of test techniques and formulas for calculating mechanical properties according to the ASTM and ISO standards.

The Rockwell hardness measurement was carried out with a hardness measuring device ITBRV-187.5-M (Moscow, Russia) by pressing the diamond cone into the surface with a pressure of 1600 MPa and a time of pressing of 15 s. Cross-sections were made on the samples; for obtaining valid results, hardness was measured five times, with the mean value being estimated.

3. Results and Discussion

Copper and aluminum powders, as well as an alloy powder of Ti-6Al-4V were used for the fabrication of the samples. The elemental composition of the powders is presented in Table 1. The particles of Ti-6Al-4V are of spherical shape and have the size d = 30 ± 20 μm (Figure 1a). The SEM images of the initial Ti-6Al-4V alloy particles, which were the main components of the samples, were processed using the software Axio Vision 4.3 (Carl Zeiss, Baden-Württemberg, Germany) based on the obtained data, their size distribution was plotted. The average diameter of the powder particles was d = 30 ± 20 μm, the particle distribution almost obeys the normal law, which corresponds to the requirements for the initial material for the SLM process. The Al nanopowder is stabilized with palmitic acid in the amount of 10 wt.%, being of spherical shape and having the diameter d = 80 ± 20 nm (Figure 1b). The Cu electrolyte powder is of dendrite shape and has the following dimensions: l_{cp} = 75 ± 25 μm, h_{cp} = 25 ± 5 μm (Figure 1c).

Table 1. The elemental composition of the initial powders, wt.%.

Ti-6Al-4V	Ti	V	Al	Fe	O
	86.45–90.9	3.5–5.3	5.3–6.8	to 0.6	to 0.02
Cu	Cu	O	S	Pb	Fe
	99.0–99.95	-	-	-	0.1–0.4
Al	Al	Al_2O_3	palmitic acid		
	85–87	5–7	8–10		

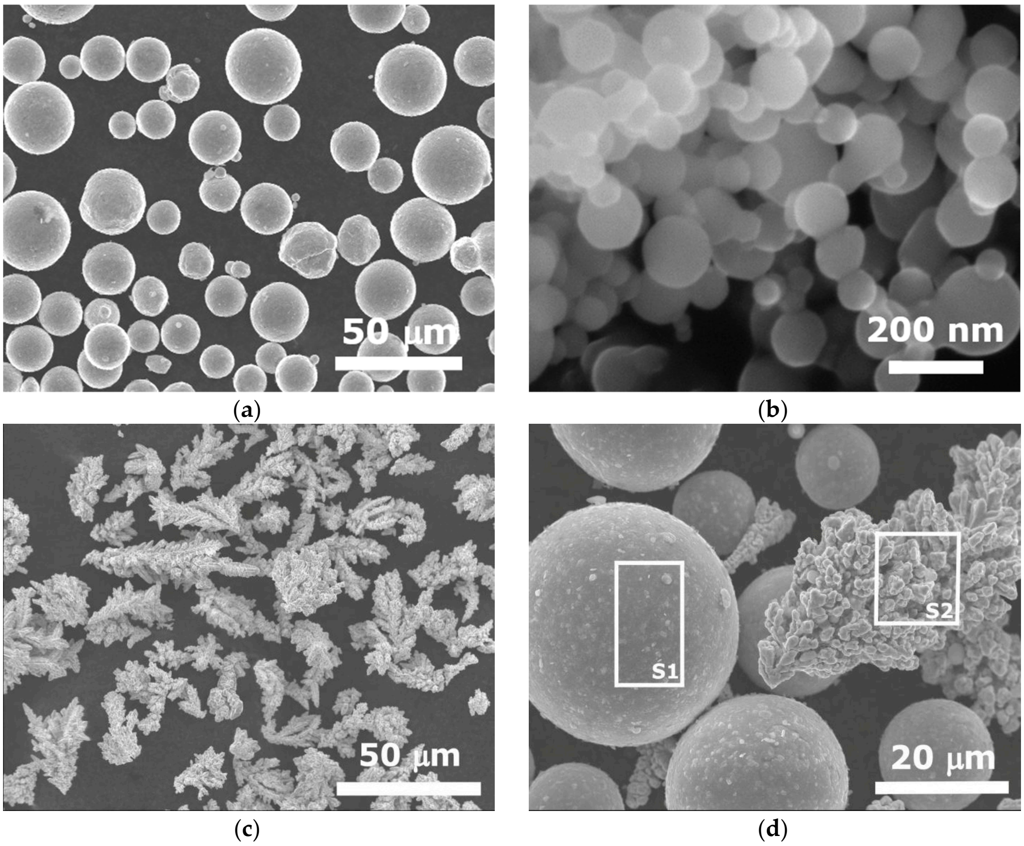

Figure 1. The SEM images of the initial powders: (**a**) Ti-6Al-4V; (**b**) Al; (**c**) Cu, (**d**) the mixture of the powders (Ti-6Al-4V)-(Cu-Al) with the indicated areas for the composition analysis. S1, S2 show the location of the elemental composition determination.

The required microstructure parameters of the obtained material are formed, depending on the SLM modes, shape, and size of the powders, character of their thermodynamic interaction, etc. The SLM method usually uses spherical powders of the same chemical composition. The simultaneous application of powders that are different in composition, density, shape, and size can result in residual porosity and, as a consequence, in a change in the physico-mechanical properties. In our case, due to the difference in shape, size, and density of the initial powders, the mixture was prepared in two stages: first, the Cu and Al powders were mixed in the ratio Cu:Al = 95:5 (wt.%) for 20 min. During the second stage, the 10 wt.% mixtures of the Cu-Al powder and 90 wt.% of the Ti-6Al-4V powder were mixed into a uniform compound for 30 min using a vibration ball mill. The percentage ratio between Ti-6Al-4V and Cu was chosen based on the analysis of the data presented in [24,26–28,30,32,35]; the authors doped the Ti-6Al-4V alloy with copper in an amount from 0.6 to 15 wt.%. Doping with aluminum nanopowder in the amount of 0.5 wt.%, in our opinion, allows us to obtain dispersed inclusions of the copper-based solid solutions, which will be located in the grains of eutectoid mixtures.

The powder mixture consists of spherical particles of Ti-6Al-4V and dendrite Cu particles, with aluminum nanoparticles being distributed on their surface during mixing (Figure 1d). The uniform distribution of aluminum is confirmed by the chemical composition estimated by EDS on the surface of the Ti-6Al-4V and Cu particles. In spectrum 1 (Table 2), obtained on the surface of the Ti-6Al-4V particle, the Al content is ≈8 wt.%; however, in the alloy it amounts to ≈6 wt.%. For the sample composition in spectrum 2 (Table 2), aluminum is also shown to be present on the particle surface in the amount of ≈18 wt.%. This allows one to draw the conclusion that the small particles on the surface of the Ti-6Al-4V and Cu powders represent aluminum. The developed specific surface of the dendrite Cu particles allows Al nanoparticles to be efficiently distributed inside the dendrites, which can provide a sufficient rate of the exothermal reaction for the formation of the Cu-Al solid solution. As a result, dispersed inclusions of the Cu-Al solid solution are formed in the intermediate layers. In the process of mixing, there occurs the formation of combinations of (Ti-6Al-4V)–Al and Cu-Al powders, which allows the components in the three-phase mixture to be uniformly distributed upon filling the chamber of a device for 3D printing and a homogeneous structure to be formed during laser melting.

Table 2. The elemental composition of the spectra obtained from the mixture of the powders of (Ti-6Al-4V)–Al, Cu-Al, wt.%.

Number of the Spectrum	Al	Ti	V	Cu	Total
1	8.04	87.89	4.07	0	100.00
2	17.73	3.45	0	78.82	100.00

The SLM modes are chosen based on the analysis of the data presented in [5,16–19,22]. During the sample fabrication by the SLM method, the laser spot diameter (d) was 170 and 190 µm, the power P varied from 225 to 350 W with the step of 25 W, and the powder layer thickness was 50 µm. The speed of laser motion was constant and amounted to 350 mm/s. The present study considers the influence of the laser spot diameter and laser power on the microstructure and properties of the obtained samples.

The mechanical properties are structurally sensitive and depend on the defects typical for materials obtained by the SLM method, such as pores and cracks. For compounds produced by the SLM technology, the presence of residual porosity is typical. The hardness and porosity of the samples obtained with a spot diameter of 190 µm and with different laser power are presented in Figure 2. In the case of close values of the sample porosity, the difference in the values of hardness can be due to the non-uniform distribution of the phases in the structure. Moreover, the mixture of the initial powders used included powders of different shapes, sizes, and densities. The aluminum particles of spherical shape and the dendrite particles could have been insufficiently uniformly distributed relative to the Ti-6Al-4V particles; the indenter could have detected either groups of grains that consisted of intermetallic compounds having high hardness, a large pore, or an agglomeration of small pores.

As follows from the curve (Figure 2), the density of the samples is less sensitive to the laser power at 325 and 350 W. In the low laser power region (lower than 300 W), the energy density in the SLM process is not high enough for the particles to be completely melted, and the width of the melt pool is small, which leads to insufficient fusion between the powder layers and to the formation of pores (Figure 3a). This was the reason for incompletely melted powder particles being detected in the pores between the scanned layers in the samples obtained at d = 170 µm and P = 225 W (Figure 3b). The analysis of the microstructure, porosity, and hardness made it possible to determine the optimum SLM mode for obtaining samples from the alloy powders and mixtures (Cu-Al). A higher density (4.96 g/cm^3) and minimum porosity (1.5%) were obtained at P = 325 W and d = 190 µm (Figure 3c).

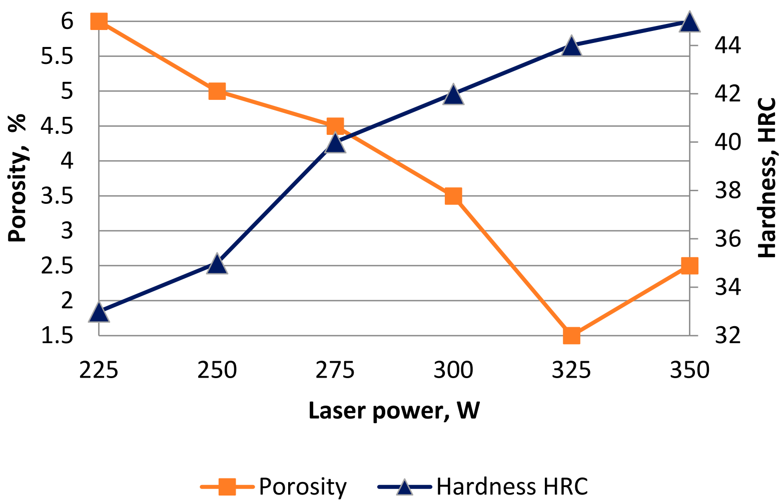

Figure 2. The dependence of the hardness and porosity of the samples (Ti-6Al-4V)-(Cu-Al) on the laser power (*d* = 190 μm).

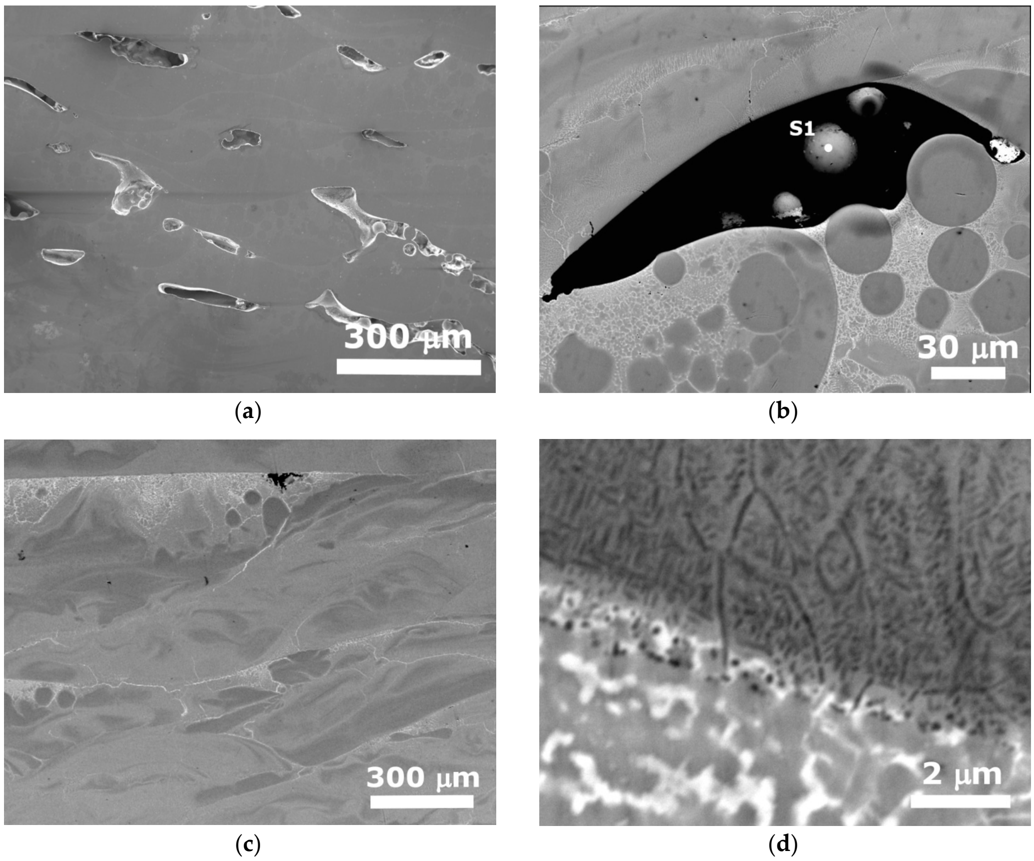

Figure 3. The SEM images of the sample microstructure: (**a**) with large interlayer pores (*d* = 170 μm, *P* = 225 W); (**b**) with the analyzed region of the particle content in an interlayer pore (*d* = 170 μm, *P* = 225 W); (**c**) general layout of the optimum structure (*d* = 190 μm, *P* = 325 W); and (**d**) with small gas pores (*d* = 190 μm, *P* = 325 W). S1 shows the location of the elemental composition determination.

Pores of two types were detected in the samples. Large pores were formed along the previous melted and crystallized layer as a result of the incomplete melting of the powder of the new layer (Figure 3a). Small gas pores were formed due to the incomplete release of gases from the melt during laser melting (Figure 3d). Pores of the first type have an elongated shape and large size, from 10 to 200 μm in length (Figure 3a), sometimes with unmelted particles inside (Figure 3a,b). The elemental composition of spectrum 1 (Figure 3b and Table 3) corresponds to Ti-6Al-4V. Pores of the second type have a diameter from 10 to 100 nm and a round shape (Figure 3d). Pores of both types are present in the samples obtained in all the SLM modes, but their number is small at *P* = 325 W and *d* = 190 µm, and their size is less than 20 µm (Figure 3c). Non-uniform areas containing a layered structure that included waves with a height of 50–100 µm were detected in the image of the microstructure of the Ti-6Al-4V alloy upon the addition of the 10% Al-Cu mixture into its composition (Figure 3c). The layer-by-layer fabrication of samples by SLM results in multiple heat cycles in the layer that crystallized earlier and, as a consequence, to the appearance of the wave-shaped layered structure.

Table 3. The elemental composition of an unmelted particle in an interlayer pore.

Elemental Composition	wt.%	at.%
Al	6.14	10.42
Ti	90.23	86.31
V	3.64	3.27

For the samples Ti-6Al-4V and 90%(Ti-6Al-4V)–10%(Cu-Al), obtained by SLM at *P* = 325 W and *d* = 190 µm, 3-point bending tests were carried out to estimate the strength and elastic modulus (Table 4).

Table 4. The mechanical properties of the samples based on Ti-6Al-4V.

Composition	Elastic Modulus, GPa	Bending Strength, MPa	Hardness, HRC	Hardness, HB	Reference
Ti-6Al-4V (casting)	-	1816	-	-	[35]
Ti-6Al-4V (SLM)	128	948	-	-	[33]
Ti-6Al-4V (SLM)	39	1300	29	300	This study
90%(Ti-6Al-4V)–10%(Cu-Al) (SLM)	50	1550	45	390	This study

Our results show that the introduction of the Cu-Al mixture into Ti-6Al-4V allows an increase in the elastic modulus by ≈25% and those of the bending strength by ≈20%, as compared to the samples of the Ti-6Al-4V composition. The sample deformation amounts to 3.5 ± 0.1%. The increase in strength is associated with the presence of the eutectoid mixture and its high dispersion in the (Ti-6Al-4V)–(Cu-Al) samples. The decrease in ductility is apparently caused by the presence of dispersed Ti_2Cu particles in the primary β-Ti grains [27,30,36]. The analysis of the surface of typical fractures of the samples (Figure 4) shows a mixed type of destruction, namely a quasi-plastic one. On the fracture surfaces, fragments were identified showing both brittle (Figure 4a) and ductile fractures (Figure 4b).

The study of the microstructure using the BSE method allows one to identify phases containing elements with different atomic numbers. The phase containing light elements has a dark gray color, while the phase containing heavier elements has a light gray color. This distribution of elements is confirmed by EDS mapping of the sample obtained at *P* = 250 W and *d* = 170 µm (Figure 5). In Figure 5a, one can clearly see incompletely melted particles of the Ti-6Al-4V alloy of a dark gray color (Figure 5b,c), surrounded by a light gray interlayer. The interlayer contains evenly distributed copper (Figure 5d). In addition, cracks were detected in the sample (Figure 5a), which may be due to the high cooling rate during SLM and too rapid crystallization. The presence of the incompletely melted particles and cracks allows making an indirect conclusion that the SLM parameters *P* = 250 W and *d* = 170 µm are not sufficient to obtain high-quality materials of this composition.

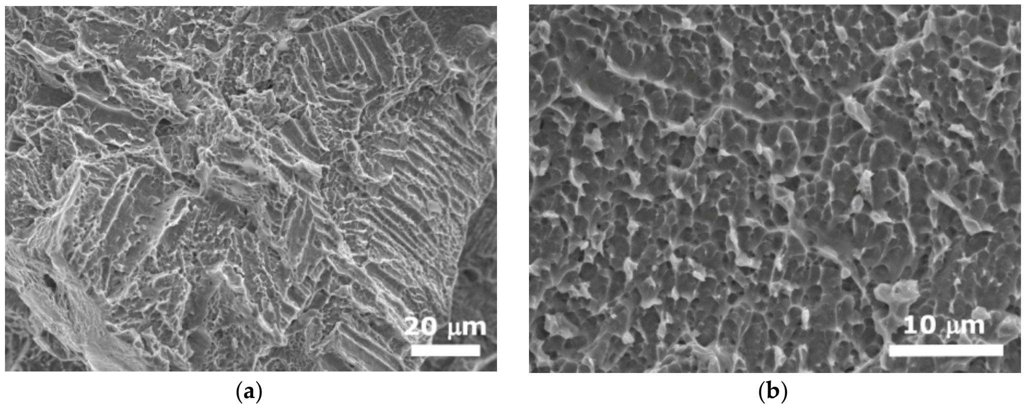

Figure 4. The SEM images of the surface of the (Ti-6Al-4V)–10(Cu-Al) samples obtained at P = 325 W and d = 190 µm after the bending tests: (**a**) brittle fracture; (**b**) ductile fracture.

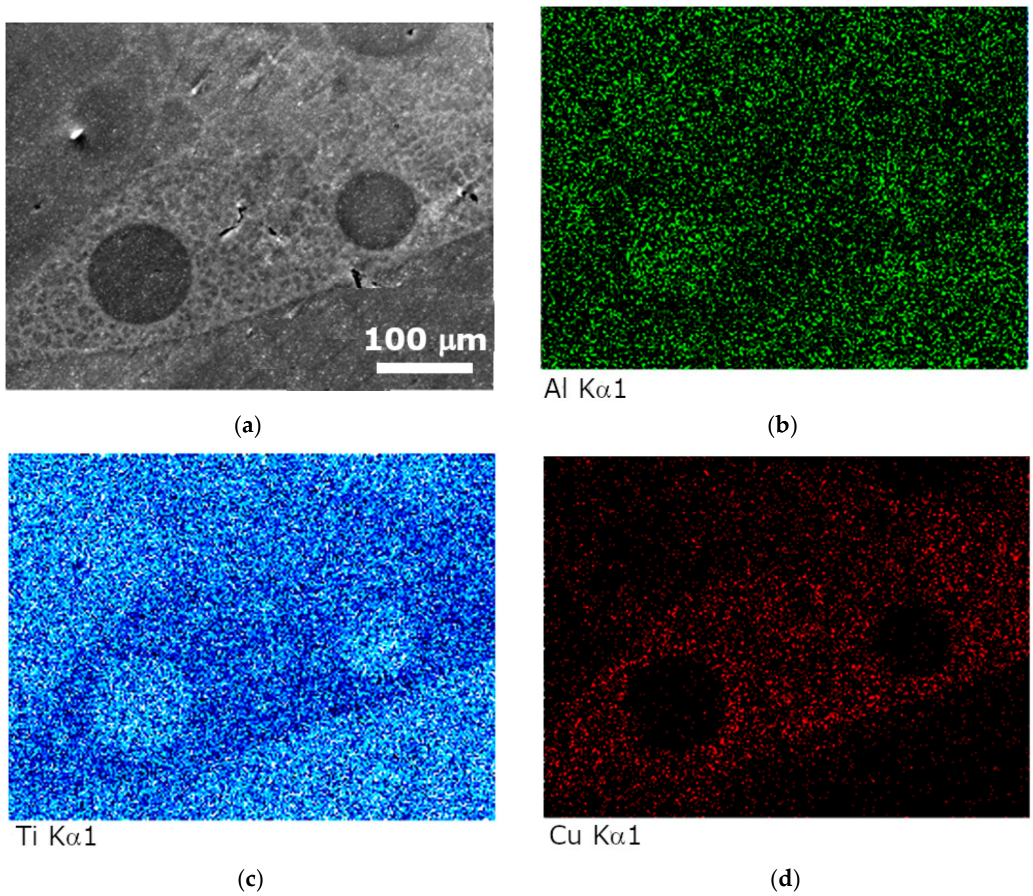

Figure 5. The SEM image/EDS mapping of Ti-6Al-4V-(Cu-Al) obtained at P = 250 W and d = 170 µm: (**a**) BSE image; (**b**–**d**) EDS mapping, Al, Cu, Ti.

The introduction of Cu-Al into the Ti-6Al-4V alloy promotes the transformation of the shape of the α-Ti and β-Ti grains from the columnar to a more equiaxed one and greater grain size distribution due to the accelerated development of the constitutional supercooling area. Layer-by-layer fabrication of samples using SLM results in multiple thermal cycles above and below the eutectoid reaction temperature (792 °C) in the previously crystallized layer. At the same time, the cooling rate of β-Ti decreases, which most likely prevents the martensitic transformation and formation of the α′-phase and promotes the transformation β-Ti→α-Ti + Ti_2Cu [36–38]. SLM provides a relatively constant cooling rate of the alloy, leading to the formation of a more uniform microstructure (Figure 6a), regardless of the size of the sample. The sufficiently high cooling rate promotes the formation of eutectoid mixtures consisting of thin plates located between the equiaxed α-Ti and β-Ti grains. Based on the BSE image analysis (Figure 6b), one can conclude that the light-colored plates contain the main amount of copper, most likely Ti_2Cu, with darker α-Ti plates located between them. The distance between the Ti_2Cu plates, i.e., the width of the α-Ti phase in the samples obtained by SLM, is 50 ± 20 nm (Figure 6b). It is known that after heat treatment of the cast material a similar structure is formed; however, the width of the α-Ti phase is about 150 nm, and after cooling in a furnace it amounts to ≈1 μm [39]. This is due to the interplate distance being dependent on the distance over which the atoms diffuse, and this distance is limited by the high cooling rate upon SLM.

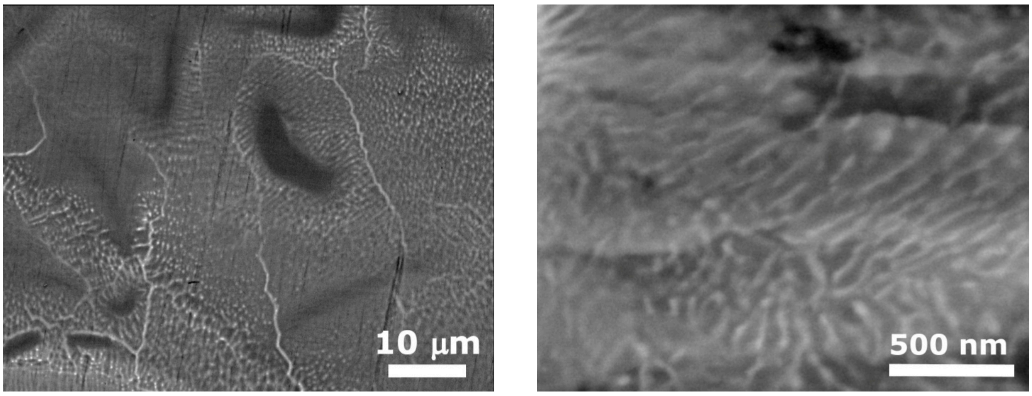

(**a**) (**b**)

Figure 6. The BSE image of the general view of microstructure of the samples (Ti-6Al-4V)–(Cu-Al), (P = 325 W and d = 180 μm) (**a**) and eutectoid mixture from the dispersed plates α-Ti and Ti_2Cu (**b**).

The elemental composition of the sample phases was studied by analyzing the data obtained by the EDS method and taking into account the phase diagrams [40]. A typical BSE image of the microstructure is shown in Figure 7a, while the concentration distribution of chemical elements along the line with a step of 10 μm is given in Figure 7b. The elemental composition of the spectra is presented in Table 4. The sharp peaks in the concentration curves (Figure 7b) allow one to conclude that the composition obtained at these points corresponds to the intermetallic compound formed. These peaks of Cu and Ti can be observed at a point of spectrum 2 (Table 4), which was acquired for the light gray plate. The composition of the phases, represented by spectra 3 and 4, is close to the composition of Ti-6Al-4V, in which up to 1.8 wt.% Cu is dissolved. It is shown in [27,39] that the solubility of copper in α-Ti reaches 1.8 wt.%, while in β-Ti, it amounts to 6.6 wt.%.

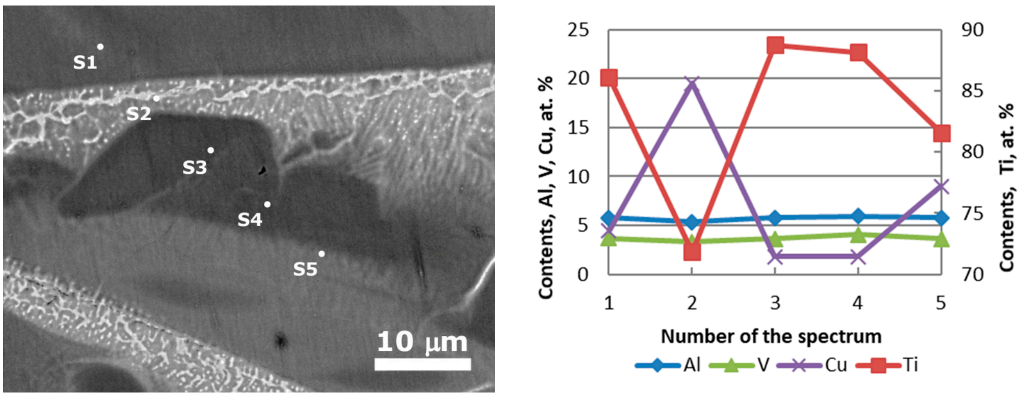

(**a**) (**b**)

Figure 7. The BSE image (**a**) and concentration curves of the element distribution along the scanning line of the composition (**b**) of the sample (Ti-6Al-4V)–(Cu-Al). S1–S5 show the location of the elemental composition determination.

For a more accurate characterization of the dispersed phases having a size smaller than 0.5 μm, the elemental composition was determined directly from the dark and gray regions (Figure 8). It should be noted that the region of generation of characteristic X-ray radiation is 1.5–2 μm, which is significantly larger than the size of the dispersed phases, and therefore, all the chemical elements included in the composition of this material are present in the spectra (Table 5).

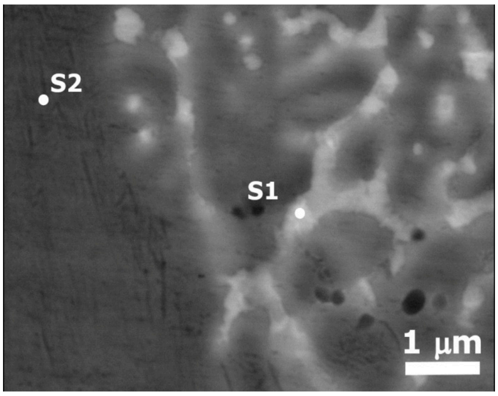

Figure 8. The SE image of the sample (Ti-6Al-4V)–(Cu-Al) with the highlighted areas of the detected elemental composition. S1, S2 show the location of the elemental composition determination.

Table 5. The elemental composition of the sample (Ti-6Al-4V)–(Cu-Al).

Number of the Spectrum	Al		Ti		V		Cu	
	wt.	at.	wt.	at.	wt.	at.	wt.	at.
1	4.46	8.35	58.47	61.74	1.99	1.98	35.09	27.93
2	5.91	10.19	85.13	82.64	3.44	3.14	5.51	4.03

The elemental composition of the phase, represented by spectrum 2, is close in composition to the Ti-6Al-4V alloy, in which 5.5 wt.% Cu is dissolved. The analysis of the composition of spectrum 1 (see Figure 8) shows a significant decrease in the titanium content, compared to the Ti-6Al-4V alloy, as well as 35 wt.% Cu. Based on the fact that the region of the signal generation significantly exceeds the size of the light phase for which spectrum 1 was obtained, its elemental composition also includes the composition of the dark phase (see spectrum 2). Thus, spectrum 1 can be assumed to consist of the Ti_2Cu phase and Al solid solution in Cu (light phase) and Ti-6Al-4V (dark phase), with 5.5 wt.% Cu being dissolved. The obtained phase composition is confirmed by the data of X-ray phase analysis. The dispersed inclusions of the Al solid solution into Cu located between the particles of Ti_2Cu (see Figure 8; Table 5, Spectrum 1) result in the particle size reduction in the intermetallic compounds, which leads to an increase in the strength of the obtained material (see Table 4).

Figure 9 shows the X-ray diffraction patterns of the Ti-6Al-4V powder, mixture of (Ti-6Al-4V)–(Cu-Al) powders, and (Ti-6Al-4V)–(Cu-Al) sample obtained by the SLM method. The analysis of the X-ray diffraction patterns revealed the presence of the α-Ti and β-Ti phases in all the samples (Figure 9a–c). The presence of copper was confirmed in the mixture of the powders (Ti-6Al-4V)–(Cu-Al) (Figure 9b), and in the sample obtained by the SLM method, the α-Ti, β-Ti and Ti_2Cu phases were identified.

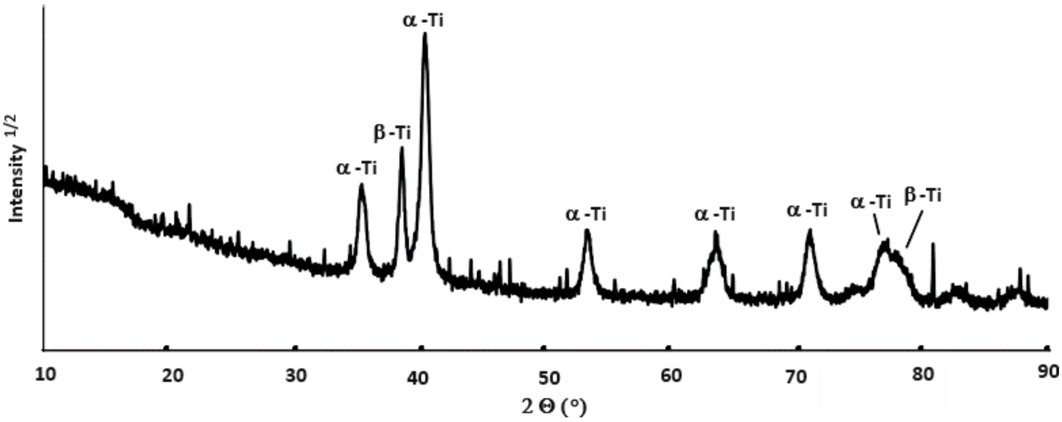

(**a**)

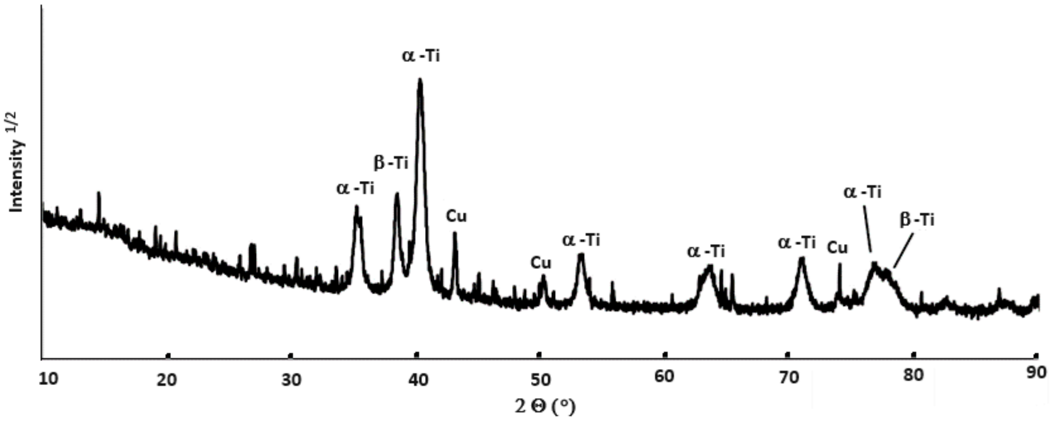

(**b**)

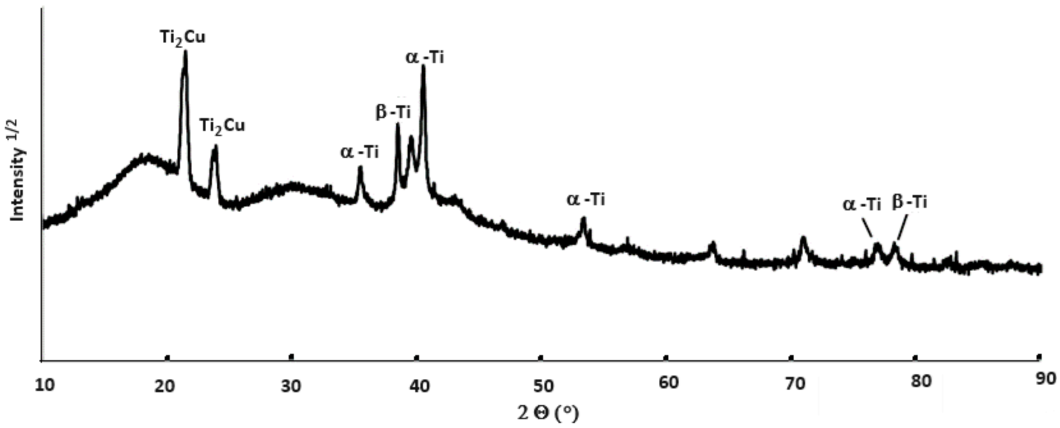

(**c**)

Figure 9. The X-ray diffraction patterns of (**a**) powder Ti-6Al-4V, (**b**) powder mixture (Ti-6Al-4V)–(Cu-Al), and (**c**) SLM (Ti-6Al-4V)–(Cu-Al).

The results obtained using the XRD method confirm that the structure of the (Ti-6Al-4V)–(Cu-Al) alloy obtained by the SLM method is formed by the phases α-Ti, β-Ti, and a eutectoid mixture of α-Ti and Ti_2Cu.

4. Conclusions

The effect of adding a 10% mixture (95% Cu-5% Al) on the physical and mechanical properties, microstructure, elemental, and phase composition of the 90%(Ti-6Al-4V)–10%(Cu-Al) alloy obtained by the SLM method was studied.

The main results are as follows:

(1) In the case of doping the Ti-6Al-4V alloy with an additive of 10 wt.% (95% Cu-5%Al), samples without fractures and large pores were obtained. Higher density and minimum porosity of 1.5 ± 0.1% were obtained at laser power of 325 W and a laser spot diameter of 190 µm, which is a feasible SLM mode for Ti-6Al-4V alloys doped with 10 wt.% (95% Cu-5%Al).
(2) The addition of 10% (Cu-Al) led to a change in the microstructure: a decrease in the grain size and the transformation of the columnar shape of the α-Ti and β-Ti grains into a more equiaxed one. The structure of the 90%(Ti-6Al-4V)–10%(Cu-Al) alloy obtained by the SLM method is formed by α-Ti, β-Ti phases, dispersed phases of an Al solid solution in Cu, and a eutectoid mixture of α-Ti and Ti_2Cu. Copper was found to be partially dissolved in α-Ti and β-Ti during crystallization.
(3) Doping Ti-6Al-4V with the Cu-Al mixture led to a significant increase in the strength and hardness of the samples. The increase in strength of the (Ti-6Al-4V)-(Cu-Al) alloy may be associated with a large volume fraction of the eutectoid mixtures formed by the dispersed α-Ti and Ti_2Cu plates.

The results presented in the given study show Cu-Al to be a promising dopant in developing high-strength alloys based on Ti for applications in the production of parts of jet and car engines, implants for medicine, and corrosion-resistant parts for chemical industry, etc. It can be assumed that increasing the amount of additionally introduced aluminum and simultaneously decreasing the amount of copper with the component ratio of 90% (Ti-6Al-4V)–10%(Cu and Al) allows us to obtain a more uniform microstructure and increasing the strength of the material.

Author Contributions: Conceptualization, G.M.Z. and Y.I.G.; methodology, M.Y.K. and E.V.G.; investigation, G.M.Z., A.K.A., E.V.G. and Y.I.G.; resources, E.V.G., M.Y.K. and E.G.Z.; writing–original draft preparation, G.M.Z., Y.I.G., A.K.A., E.V.G. and S.M.Z.; writing–review and editing, G.M.Z. and S.M.Z.; visualization, E.G.Z. All authors have read and agreed to the published version of the manuscript.

Funding: This research received no external funding.

Data Availability Statement: The original contributions presented in the study are included in the article. Further inquiries can be directed to the corresponding authors.

Acknowledgments: The SEM and EDS investigations were conducted in the laboratory of electron microscopy of the SFU Joint Scientific Center. S.M. Zharkov thanks for financial support the state assignment of Kirensky Institute of Physics. The authors would like to thank A.N. Shchelkanov, director of the company Polihrom, for providing the opportunity to use the ASTRA 420 printer.

Conflicts of Interest: Author Evgeny V. Gerasimov was employed by the company Polihrom. The remaining authors declare that the research was conducted in the absence of any commercial or financial relationships that could be construed as a potential conflict of interest.

References

1. Yap, C.Y.; Chua, C.K.; Dong, Z.L.; Liu, Z.H.; Zhang, D.Q.; Loh, L.E.; Sing, S.L. Review of selective laser melting: Materials and applications. *Appl. Phys. Rev.* **2015**, *2*, 041101. [CrossRef]
2. Harun, W.S.W.; Manam, N.S.; Kamariah, M.S.I.N.; Sharif, S.; Zulkifly, A.H.; Ahmad, I.; Miura, H. A review of powdered additive manufacturing techniques for Ti-6al-4v biomedical applications. *Powder Technol.* **2018**, *331*, 74–97. [CrossRef]
3. Tiwari, S.K.; Pande, S.; Agrawal, S.; Bobade, S.M. Selection of selective laser sintering materials for different applications. *Rapid Prototyp. J.* **2015**, *21*, 630–648. [CrossRef]
4. Sachdeva, A.; Singh, S.; Sharma, V.S. Investigating surface roughness of parts produced by SLS process. *Int. J. Adv. Manuf. Technol.* **2013**, *64*, 1505–1516. [CrossRef]
5. Maitra, V.; Shi, J. Evaluating the predictability of Surface Roughness of Ti-6Al-4V alloy from selective laser melting. *Adv. Eng. Mater.* **2023**, *25*, 2300075. [CrossRef]
6. Dallago, M.; Zanini, F.; Carmignato, S.; Pasini, D.; Benedetti, M. Effect of the geometrical defectiveness on the mechanical properties of SLM biomedical Ti6Al4V lattices. *Procedia Struct. Integr.* **2018**, *13*, 161–167. [CrossRef]
7. Liović, D.; Franulović, M.; Kozak, D. The effect of process parameters on mechanical behavior of selective laser melted Ti6Al4V alloy. *Procedia Struct. Integr.* **2023**, *46*, 42–48. [CrossRef]

8. Sutton, A.T.; Kriewall, C.S.; Leu, M.C.; Newkirk, J.W. Powders for additive manufacturing processes: Characterization techniques and effects on part properties. In Proceedings of the 27th Annual International Solid Freeform Fabrication Symposium, University of Texas at Austin, Austin, TX, USA, 8–10 August 2016; pp. 1004–1030. Available online: https://scholarsmine.mst.edu/mec_aereng_facwork/3694/ (accessed on 20 July 2024).
9. Slotwinski, J.A.; Garboczi, E.J.; Stutzman, P.E.; Ferraris, C.F.; Watson, S.S.; Peltz, M.A. Characterization of metal powders used for additive manufacturing. *J. Res. Natl. Inst. Stand. Technol.* **2014**, *119*, 460. [CrossRef] [PubMed]
10. Capus, J. Titanium powder developments for AM–A round-up. *Met. Powder Rep.* **2017**, *72*, 384–388. [CrossRef]
11. Anderson, I.E.; White, E.M.; Dehoff, R. Feedstock powder processing research needs for additive manufacturing development. *Curr. Opin. Solid State Mater. Sci.* **2018**, *22*, 8–15. [CrossRef]
12. Liu, Q.; Wang, Y.; Zheng, H.; Tang, K.; Ding, L.; Li, H.; Gong, S. Microstructure and mechanical properties of LMD–SLM hybrid forming Ti6Al4V alloy. *Mater. Sci. Eng. A* **2016**, *660*, 24–33. [CrossRef]
13. Liu, Y.J.; Li, S.J.; Wang, H.L.; Hou, W.T.; Hao, Y.L.; Yang, R.; Sercombe, T.B.; Zhang, L.C. Microstructure, defects and mechanical behavior of beta-type titanium porous structures manufactured by electron beam melting and selective laser melting. *Acta Mater.* **2016**, *113*, 56–67. [CrossRef]
14. Tan, X.; Kok, Y.; Tan, Y.J.; Descoins, M.; Mangelinck, D.; Tor, S.B.; Leong, K.F.; Chua, C.K. Graded microstructure and mechanical properties of additive manufactured Ti–6Al–4V via electron beam melting. *Acta Mater.* **2015**, *97*, 1–16. [CrossRef]
15. Zhou, B.; Zhou, J.; Li, H.; Lin, F. A study of the microstructures and mechanical properties of Ti6Al4V fabricated by SLM under vacuum. *Mater. Sci. Eng. A* **2018**, *724*, 1–10. [CrossRef]
16. Kathiresan, M.; Karthikeyan, M.; Immanuel, R.J. A short review on SLM-processed Ti6Al4V composites. *Proc. Inst. Mech. Eng. Part E J. Process Mech. Eng.* **2023**. [CrossRef]
17. Xu, W.; Lui, E.W.; Pateras, A.; Qian, M.; Brandt, M.J.A.M. In situ tailoring microstructure in additively manufactured Ti-6Al-4V for superior mechanical performance. *Acta Mater.* **2017**, *125*, 390–400. [CrossRef]
18. Sun, D.; Gu, D.; Lin, K.; Ma, J.; Chen, W.; Huang, J.; Sun, X.; Chu, M. Selective laser melting of titanium parts: Influence of laser process parameters on macro-and microstructures and tensile property. *Powder Technol.* **2019**, *342*, 371–379. [CrossRef]
19. Agius, D.; Kourousis, K.I.; Wallbrink, C.; Song, T. Cyclic plasticity and microstructure of as-built SLM Ti-6Al-4V: The effect of build orientation. *Mater. Sci. Eng. A* **2017**, *701*, 85–100. [CrossRef]
20. Yang, J.; Yu, H.; Wang, Z.; Zeng, X. Effect of crystallographic orientation on mechanical anisotropy of selective laser melted Ti-6Al-4V alloy. *Mater. Charact.* **2017**, *127*, 137–145. [CrossRef]
21. Aoki, T.; Okafor, I.C.I.; Watanabe, I.; Hattori, M.; Oda, Y.; Okabe, T. Mechanical properties of cast Ti-6Al-4V-XCu alloys. *J. Oral Rehabil.* **2004**, *31*, 1109–1114. [CrossRef]
22. Zadeh, J.M.; Yeganeh, M.; Zaree, S.R.A.; Khorasanian, M. Microstructure and corrosion behavior of Ti-10Cu fabricated by selective laser melting. *Mater. Today Commun.* **2024**, *39*, 109103. [CrossRef]
23. Yang, W.; Chen, Y.; Yang, L.; Zhu, S.; Wang, Y.; Shi, Y. Optimization of mechanical and antibacterial properties of SLM–fabricated TC4–5Cu alloy by annealing heat treatment. *J. Alloys Compd.* **2024**, *971*, 172565. [CrossRef]
24. Polozov, I.A.; Sokolova, V.V.; Gracheva, A.M.; Popovich, A.A. Influence of copper on the microstructure and mechanical properties of titanium ortho-alloy produced by selective laser melting. *Powder Metall. Funct. Coat.* **2024**, *18*, 31–39. [CrossRef]
25. Chen, Y.; Yang, W.; Zhu, S.; Shi, Y. Microstructural, mechanical and in vitro biological properties of Ti6Al4V-5Cu alloy fabricated by selective laser melting. *Mater. Charact.* **2023**, *200*, 112858. [CrossRef]
26. Goettgens, V.S.; Kaserer, L.; Braun, J.; Letofsky-Papst, I.; Mitsche, S.; Leichtfried, G. Microstructure of a modulated Ti-6Al-4V–Cu alloy fabricated via in situ alloying in laser powder bed fusion. *Materialia* **2023**, *28*, 101731. [CrossRef]
27. Goettgens, V.S.; Kaserer, L.; Braun, J.; Busch, R.; Berthold, L.; Patzig, C.; Leichtfried, G. Microstructural evolution and mechanical properties of Ti-6Al-4V in situ alloyed with 3.5 wt.% Cu by laser powder bed fusion. *Materialia* **2023**, *32*, 101928. [CrossRef]
28. Koike, M.; Cai, Z.; Oda, Y.; Hattori, M.; Fujii, H.; Okabe, T. Corrosion behavior of cast Ti-6Al-4V alloyed with Cu. *J. Biomed. Mater. Res. Part B Appl. Biomater. Off. J. Soc. Biomater. Jpn. Soc. Biomater. Aust. Soc. Biomater. Korean Soc. Biomater.* **2005**, *73*, 368–374. [CrossRef]
29. Zhou, M.; Sun, H.; Gan, Y.; Ji, C.; Chen, Y.; Lu, Y.; Wang, Q. Tuning the Corrosion Resistance, Antibacterial Activity, and Cytocompatibility by Constructing Grooves on the Surface of Ti6Al4V3Cu Alloy. *Acta Metall. Sin. (Engl. Lett.)* **2023**, *36*, 1979–1998. [CrossRef]
30. Ma, Z.; Ren, L.; Liu, R.; Yang, K.; Zhang, Y.; Liao, Z.; Liu, W.; Qi, M.; Misra, R.D.K. Effect of heat treatment on Cu distribution, antibacterial performance and cytotoxicity of Ti-6Al-4V-5Cu alloy. *J. Mater. Sci. Technol.* **2015**, *31*, 723–732. [CrossRef]
31. Ren, L.; Ma, Z.; Li, M.; Zhang, Y.; Liu, W.; Liao, Z.; Yang, K. Antibacterial properties of Ti-6Al-4V-xCu alloys. *J. Mater. Sci. Technol.* **2014**, *30*, 699–705. [CrossRef]
32. Zykova, A.P.; Nikolaeva, A.V.; Vorontsov, A.V.; Chumaevskii, A.V.; Nikonov, S.Y.; Moskvichev, E.N.; Gurianov, D.A.; Savchenko, N.L.; Kolubaev, E.A.; Tarasov, S.Y. Effect of copper content on grain structure evolution in additively manufactured Ti-6Al-4V alloy. *Phys. Mesomech.* **2023**, *26*, 107–125. [CrossRef]
33. Sun, W.; Ma, Y.E.; Zhang, W.; Qian, X.; Huang, W.; Wang, Z. Effects of the Build Direction on Mechanical Performance of Laser Powder Bed Fusion Additively Manufactured Ti6Al4V under Different Loadings. *Adv. Eng. Mater.* **2021**, *23*, 2100611. [CrossRef]
34. Shchelkanov, A.N. Device of Multi-Position Focusing of Uniform Laser Radiation for Construction of Metal Parts by Selective Laser Melting Method. Russian Patent 2771495, 5 May 2022. (In Russian).

35. Prakash, G.; Singh, N.K.; Gupta, N.K. Flow behaviour of Ti-6Al-4V alloy in a wide range of strain rates and temperatures under tensile, compressive and flexural loads. *Int. J. Impact Eng.* **2023**, *176*, 104549. [CrossRef]
36. Zhang, D.; Qiu, D.; Gibson, M.A.; Zheng, Y.; Fraser, H.L.; StJohn, D.H.; Easton, M.A. Additive manufacturing of ultrafine-grained high-strength titanium alloys. *Nature* **2019**, *576*, 91–95. [CrossRef] [PubMed]
37. Wang, X.; Zhang, L.J.; Ning, J.; Na, S.J. Effect of Cu-induced eutectoid transformation on microstructure and mechanical properties of Ti–6Al–4V alloy by laser wire deposition. *Mater. Sci. Eng. A* **2022**, *833*, 142316. [CrossRef]
38. Donthula, H.; Vishwanadh, B.; Alam, T.; Borkar, T.; Contieri, R.J.; Caram, R.; Banerjee, R.; Tewari, R.; Dey, G.K.; Banerjee, S. Morphological evolution of transformation products and eutectoid transformation(s) in a hyper-eutectoid Ti-12 at% Cu alloy. *Acta Mater.* **2019**, *168*, 63–75. [CrossRef]
39. Guo, S.; Lu, Y.; Wu, S.; Liu, L.; He, M.; Zhao, C.; Gan, Y.; Lin, J.; Luo, J.; Xu, X.; et al. Preliminary study on the corrosion resistance, antibacterial activity and cytotoxicity of selective-laser-melted Ti6Al4V-xCu alloys. *Mater. Sci. Eng. C* **2017**, *72*, 631–640. [CrossRef] [PubMed]
40. Massalski, T.B.; Okamoto, H.; Subramanian, P.R.; Kacprzak, L. (Eds.) *Binary Alloy Phase Diagrams*, 2nd ed.; ASM International: Novelty, OH, USA, 1990; 3589p, ISBN 978-0-87170-403-0.